ICEMG 2023-XXXXX

# Study of performance characteristics of a line-start synchronous reluctance motor over its synchronization region

**Ali Jamali-Fard**[1], **Mojtaba Mirsalim**[2]

[1,2]Electrical Machines and Transformer Research Laboratory (EMTRL)
[1,2]Department of Electrical Engineering, Amirkabir University of Technology, Tehran, Iran
[2]Electrical Engineering Department, St. Mary's University, San Antonio, Texas, USA
[1]a.jamalifard@aut.ac.ir, [2]mmirsalim@stmarytx.edu

## Abstract

The induction motor (IM) is by far, the most used motor type in the industry, especially for fixed-speed line-start applications. But, due to the rotor slip and joule losses of the rotor cage, IM hardly reaches high-efficiency classes. A good candidate instead of IM to reach higher efficiency classes is the line-start synchronous reluctance motor (LS-SynRM). The main design challenge of an LS-SynRM is the synchronization capability. This paper presents a detailed study of a 4kW-1500rpm LS-SynRM over its synchronization region. The performance characteristics of the case-study motor for different operating conditions are calculated by the transient finite element simulations. The aim is to provide some design guidelines regarding the extension of the synchronization region for a healthy start-up of the motor for line-start applications.

**Keywords:** Line-start, Synchronous reluctance motor, Synchronization region, Efficiency

## Introduction

The development of efficient electric motors always has widespread attention due to the steady increase in global energy demand. Among different applications, fans and pumps have a considerable share [1, 2]. The induction motor (IM) is the most used motor type for fan and pump applications [1, 3, 4]. There are several advantages for the IMs used for fan and pump applications: (i) robust rotor structure, (ii) line-start ability, (iii) low maintenance, (iv) low noise and vibration, (v) low cost, (vi) fault tolerant.

One disadvantage of IM is the rotor slip. Because of joule losses of the rotor cage, IM hardly reaches high-efficiency classes (in sense of commercial design) [5]. Several alternatives for IMs were investigated to increase the efficiency of electric motors used for fan and pump applications. A suitable alternative is a line-start synchronous motor. The rotor of a line-start synchronous motor revolves at synchronous speed, and there are no conductive losses on it. This feature makes the rotor of a line-start synchronous motor cooler than the rotor of an induction motor. Several line-start synchronous motor structures either with or without permanent magnets (PMs) were developed [6-8]. The line-start interior PM motor is a good candidate which can reach the IE5 efficiency class. But extensive use of this motor type is limited due to fluctuations in the magnet price. In addition, when using the strong magnets in this motor type, braking torque during the start-up increases which can impede a healthy start-up of the motor.

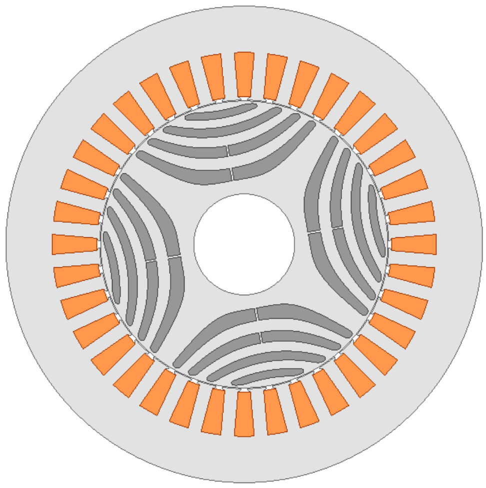

Figure 1. Structure of the case-study motor

Line-start synchronous reluctance motor (LS-SynRM) is a suitable alternative for IM for fixed-speed applications [9-11]. Unlike line-start PM motors, the rotor core of an LS-SynRM is magnet free, and there is no braking toque during the start-up. The material composition of the rotor core of LS-SynRM is similar to IM. Figure 1 shows the structure of an LS-SynRM. The stator core is slotted, and the stator core is integral slot distributed winding (ISDW). The rotor core contains several flux-barrier layers per pole, and they are filled with a conductive material (For example, aluminum).

This paper deals with the challenges in the rotor design of a case-study LS-SynRM regarding a healthy start-up. Several cases are studied to investigate motor performance and find the relationship between the design parameters of the rotor core and the synchronization region. The geometry of the generated rotor cores in this work are based on the method presented in [12].The ANSYS Maxwell software is used for transient finite element simulations. Performance characteristics of the studied rotor cores are presented and discussed.

Table 1. Specifications of the case-study motor

| Parameter | Value |
|---|---|
| Rated output power | 4kW |
| Rated speed | 1500rpm |
| Rated torque | 25Nm |
| Supply voltage | 400V |
| Terminal current | 8.3A |
| Stator bore diameter | 104mm |
| Outer stator diameter | 170mm |
| Stack length | 135mm |

**Case-study motor specifications**

The electrical and mechanical specifications of the case-study motor are given in Table 1. The rated torque of the motor is 25Nm. For a correct transient simulation of the motor start-up, the exact torque-speed curve of the load should be considered in coupled circuit, field, and motion equations. Thanks to ANSYS Maxwell software, the load torque could be applied as a function of the rotor speed in dynamic simulations. The target application considered in this paper is a pump. The torque-speed curve of a pump can be modeled by a quadratic equation,

$$T_L = k_L \times \omega^2 \quad (1)$$

Here, $T_L$ is the load torque, $k_L$ is the load constant, and $\omega$ is the mechanical angular speed of the rotor.

In all dynamic simulations, performed in this work, the quadratic equation is used for applying the load torque. The load constant can be calculated by the following formula:

$$k_L = \frac{T_{\text{rated}}}{\omega_s^2} \quad (2)$$

Here, $T_{\text{rated}}$ is the rated torque which is equal to 25Nm and $\omega_s$ is the synchronous mechanical angular speed.

**Components of the electric torque**

There are two electromagnetic torque types during the start-up of an LS-SynRM:

- Induction torque
- Reluctance torque

The induction torque is due to the interaction of the stator field with induced eddy currents inside the flux-barrier layers of the rotor core. The reluctance type is because of magnetization and magnetic anisotropy of the rotor core. The value of the reluctance torque is proportional to the level of rotor magnetic anisotropy known as the saliency ratio which is defined as the ratio of the direct axis inductance per quadrature axis inductance while the d-axis of the rotor core is considered along with the minimum reluctance path.

In an LS-SynRM, Like IM, the average value of induction torque is not zero for all speeds except the synchronous speed. On the other hand, the only non-zero average value for reluctance torque occurs at the synchronous speed, and for the rest speeds, the average value of the reluctance torque is equal to zero. A healthy start-up is when the motor can pass positive and negative cycling reluctance torques before the synchronous speed by induction torque.

The design process and sizing of an LS-SynRM are similar to a SynRM. The only difference is adding some conductive parts inside the rotor core to generate the induction torque for the line-start application. In this work, a 4kW-1500rpm commercial induction motor is considered a benchmark. The sizing of the stator core of the case-study motor is done similarly to the benchmark induction motor by assuming values for the magnetic loading and electric loading close to the benchmark motor.

**Synchronization region**

Synchronization of an LS-SynRM depends on the following factors:

- Supply voltage decrease
- Rotor moment-of-inertia
- Overload
- Stator resistance
- The temperature of rotor conductive parts

Among the above factors, the supply voltage decrease has the most destructive effect because the induction torque is a function of supply voltage squared. Rotor moment-of inertia is the second important influencing factor. When the rotor moment-of-inertia increases, the negative acceleration due to negative reluctance torque cycles before the synchronous speed increases. By increasing the amount of this negative acceleration, the rotor cannot reach the synchronous speed and start fluctuating.

Among all factors, supply voltage decrease and the rotor moment-of-inertia could be used as deterministic parameters. Therefore, an operating region on the plane of supply voltage decrease and rotor moment-of-inertial could be analyzed to investigate the synchronization capability of an LS-SynRM.

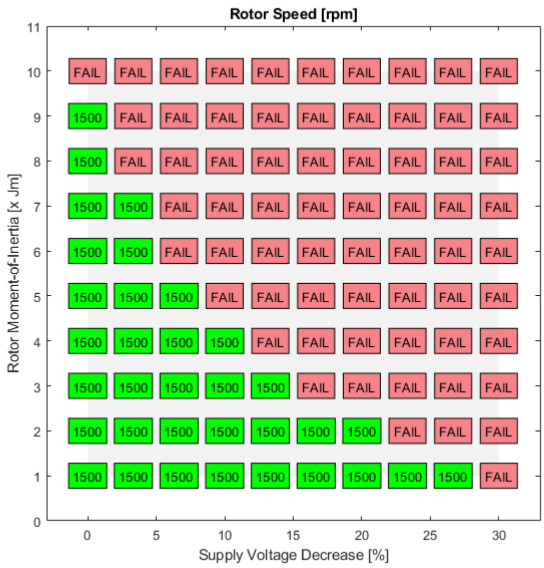


Figure 2. The synchronization region of an LS-SynRM

Figure 2 shows an example of the synchronization region. In this figure, the value of the steady-state speed for different values of the supply voltage decrease and the rotor moment-of-inertia are shown. The x-axis is the supply voltage decrease in percentage, and the y-axis is a multiplication of the rotor moment-of-inertia. Green rectangles show the operating points with successful synchronization, and red rectangles show the operating point with the failure in synchronization. As it can be seen, by increasing the value of supply voltage decrease or rotor moment-of-inertia the synchronization capability decreases. The green region is known as the synchronization region.

**Results and Discussion**

*(a) The effect of the air insulation ratio*

The design of an LS-SynRm starts with sizing the stator core considering the rated operation of the motor. Then, this seed motor could be optimized for maximum torque, efficiency, and power density. The next step is the modification of the rotor core to get a minimum torque ripple and to add the line-start ability. Detailed design and optimization of SynRM are presented in [13, 14]. This work aims to investigate the effect of one of the important rotor parameters of the rotor core, known as the air insulation ratio, on the synchronization capability of the case-study LS-SynRM.

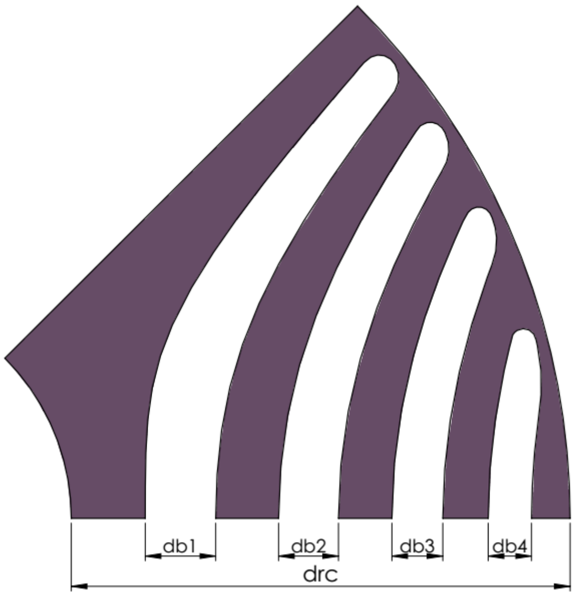


Figure 3. Half pole of the rotor core of the case-study motor

The air insulation ratio is defined as the ratio of the total thickness of flux-barrier layers (summation of the depth of flux-barrier layers) per depth of the rotor core. Figure 3 shows half the pole of the rotor core. The numbering of flux-barrier layers is from the innermost layer to the outermost layer. The air insulation ratio for this example is equal:

$$K_{air} = \frac{d_{b1} + d_{b2} + d_{b3} + d_{b4}}{d_{rc}} \tag{3}$$

Here, $d_{bi}$ is depth of the $i^{th}$ flux-barrier layer, and $d_{rc}$ is the total depth of the rotor core. The rotor core geometry in this work is generated by the method presented in [12] and optimized using the per-unit optimization model introduced in [15].

Figure 4 shows the summary of simulation results for three different values of $K_{air}$. Figures 4a, 4b, and 4c show the case-study rotor cores. The value of $K_{air}$ for these rotor cores is equal to 0.4, 0.45, and 0.5 respectively. As it is seen, when the value of shaft diameter and outer rotor radius is constant, by increasing the value of $K_{air}$, the cross-sectional area of conductive parts increases while the thickness of flux-carrier layers decreases.

Figures 4d, 4e, and 4f show the synchronization regions. As can be seen, by increasing the value of $K_{air}$, the area of the synchronization region increases. The reason is when we increase the value of $K_{air}$, the resistance of the conductive parts of the rotor decreases, and consequently, the maximum induction torque (breakdown torque) occurs at a lower slip value. Occurring the maximum torque at a lower slip is a good point because there will be enough torque to push the rotor toward the synchronous speed and synchronize the motor.

The negative aspect of increasing the value of $K_{air}$ is reducing the thickness of flux-carrier layers. By reducing the thickness of flux-carrier layers, the level of magnetic saturation in them increases. This saturation increases the value of magneto-motive force drop over the rotor core which increases the magnetizing current and reduces the motor efficiency. This effect is seen in Figures 4g, 4h, and 4i. These figures show the value of the terminal current for the synchronized points. As it is seen, the amplitude of the current increases by increasing the value of $K_{air}$. For a specific rotor core, the value of terminal current is not a function of the rotor moment-of-inertial, but it increased by the increase in the percentage value of supply voltage decrease. Figures 4j, 4k, and 4l show the motor efficiency for synchronized points.

*(b) The equation of the boundary curve*

A high number of transient simulations considering a fine step size both for supply voltage decrease and rotor moment-of-inertia have been performed to calculate the boundary of the synchronization region. The aim is to fit a curve on the synchronization boundary to find a relationship between the synchronization capability of the LS-SynRM and the supply voltage decrease and the rotor moment-of-inertia.

Figure 5 shows the synchronization region of the case-study motor when the value of the air insulation ratio is equal to 0.45. The solid line shows the boundary of the synchronization region. This boundary curve could be considered as one of the contour lines of the following function:

$$f(v_d, J_m) = \frac{K_1}{(v_d + v_{d0})^{\alpha} \times (J_m + J_{m0})^{\beta}} \tag{4}$$

Here, $f(v_d, J_m)$ is a two dimensional function. $v_d$ is the voltage decrease, $J_m$ is the rotor moment-of-inertia, and $(K_1, v_{d0}, J_{m0}, \alpha, \beta)$ are constants.

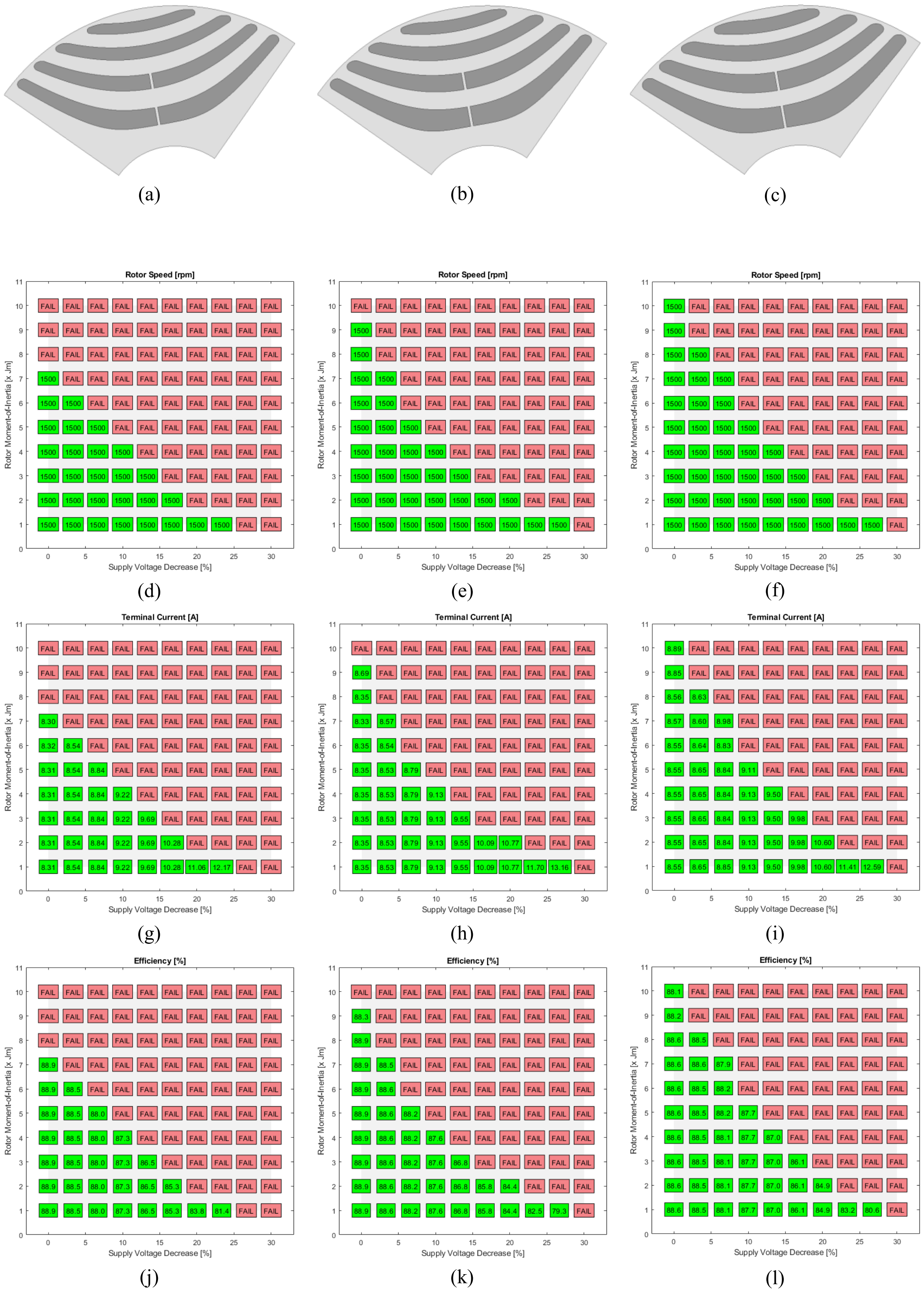


Figure 4. Simulations results, (a) (b) (c): rotor cores, (d) (e) (f): synchronization regions, (g) (h) (i): RMS value of the terminal current for synchronized points, (j) (k) (l): the value of the motor efficiency for synchronized points

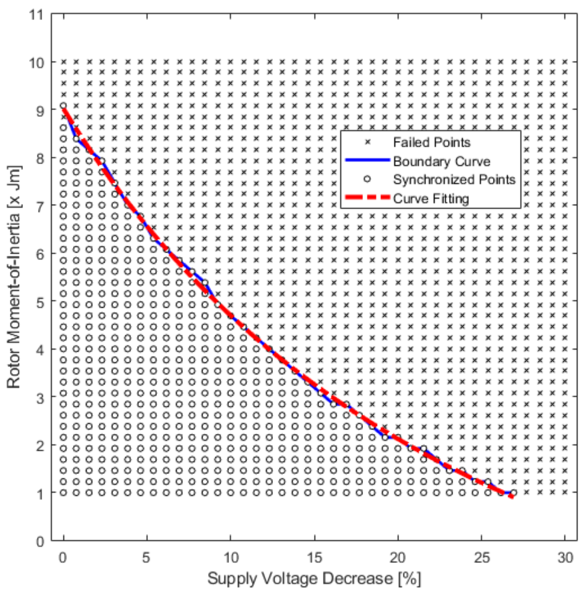

Figure 5. The boundary of the synchronization region

The boundary of the synchronization region is one of the contour lines of the function $f(v_d, J_m)$. Therefore, if we consider that the value of function $f(v_d, J_m)$ for the corresponding contour line is equal to $K_2$, we can write:

$$K_2 = \frac{K_1}{(v_d + v_{d0})^{\alpha} \times (J_m + J_{m0})^{\beta}} \Rightarrow \\ J_m = \sqrt[\beta]{\frac{K_3}{(v_d + v_{d0})^{\alpha}}} - J_{m0} \tag{5}$$

Equation 5 is a single variable function which can represent the boundary of synchronization region. The value of $K_3$ in this equation is equal:

$$K_3 = \frac{K_1}{K_2} \tag{6}$$

The MATLAB *lsqcurvefit* function is used to do curve fitting of Equation 5 in a least-squares sense over the boundary points of the synchronization region. There are five constants in Equation 5. The *lsqcurvefit* function gets the initial values for these constants and tries to fit the equation on data points. Because the induction torque is proportional to the supply voltage squared and the exponent of the rotor moment-of-inertia in the motion equation is equal to one, we considered the following initial values for $\alpha$ and $\beta$:

$$\begin{cases} \alpha = 2 \\ \beta = 1 \end{cases} \tag{7}$$

The dashed line in Figure 5 shows the derived curve that is calculated by the least square method. As can be seen, this curve has a good match with the boundary of the synchronization region. Therefore, qualitatively speaking, we can write:

$$\text{synchronization capability} \begin{cases} \propto \dfrac{1}{v_d^2} \\ \propto \dfrac{1}{J_m} \end{cases} \tag{8}$$

This means the synchronization capability of a line-start synchronous reluctance motor is proportional to the inverse of the rotor moment-of-inertia and inverse-square of the supply voltage decrease. The constant $K_3$ is proportional to the cross-section area of conductive parts of the rotor core or qualitatively speaking,

$$K_3 \propto K_{air} \tag{9}$$

## Conclusions

In this paper, a study of the performance characteristics of several rotor cores of a 4kW-1500rpm case-study line-start synchronous reluctance motor was presented. The aim was the calculation of the synchronization region to investigate the effect of the rotor air insulation ratio parameter on the synchronization capability of the motor. The synchronization region of the case studies was calculated for a range of the supply voltage decrease and rotor moment-of-inertia by transient finite element simulations. According to the results, the area of the synchronization region extended by increasing the value of the rotor air insulation ratio (because of the reduction of the resistance of rotor conductive parts). But, by increasing the value of the rotor air insulation ratio, the value of terminal current was decreased, and the motor efficiency was reduced. A trade-off in setting the value of the rotor air insulation ratio is needed in such a way that we have a good area for the synchronization region without deteriorating the steady-state performance of the motor.

The paper concluded by investigating an equation for the boundary curve of the synchronization region. This curve was calculated by performing a high number of transient simulations and then by the least-square curve fitting over the boundary of the synchronization region. It was verified that the synchronization capability of a line-start synchronous reluctance motor is proportional to the inverse of the rotor moment-of-inertia and inverse-square of the supply voltage decrease by transient finite element simulations.

## References

[1] S. Baka, S. Sashidhar, and B. G. Fernandes, "Design of an Energy Efficient Line-Start Two-Pole Ferrite Assisted Synchronous Reluctance Motor for Water Pumps," *IEEE Transactions on Energy Conversion,* vol. 36, no. 2, pp. 961-970, 2021.

[2] A. Kersten, Y. Liu, and D. Pehrman, "Rotor Design of a Line-Start Synchronous Reluctance Machine with Respect to Induction Machine for Industrial Applications," in *2018 XIII International Conference on Electrical Machines (ICEM)*, 2018, pp. 393-399.

[3] Ł. Knypiński and F. Gillon, "Sizing by optimization of line-start synchronous motor," *COMPEL - The international journal for computation and*

*mathematics in electrical and electronic engineering,* vol. ahead-of-print, no. ahead-of-print, 2021.

[4] Y. Hu, B. Chen, Y. Xiao, J. Shi, and L. Li, "Study on the Influence of Design and Optimization of Rotor Bars on Parameters of a Line-Start Synchronous Reluctance Motor," *IEEE Transactions on Industry Applications,* vol. 56, no. 2, pp. 1368-1376, 2020.

[5] D. Mingardi, N. Bianchi, and L. Alberti, "Optimal choice of stack length and conductors of line start synchronous motors," in *8th IET International Conference on Power Electronics, Machines and Drives (PEMD 2016)*, 2016, pp. 1-6.

[6] W. Fei, P. C. K. Luk, J. Ma, J. X. Shen, and G. Yang, "A High-Performance Line-Start Permanent Magnet Synchronous Motor Amended From a Small Industrial Three-Phase Induction Motor," *IEEE Transactions on Magnetics,* vol. 45, no. 10, pp. 4724-4727, 2009.

[7] A. D. Aliabad, M. Mirsalim, and N. F. Ershad, "Line-Start Permanent-Magnet Motors: Significant Improvements in Starting Torque, Synchronization, and Steady-State Performance," *IEEE Transactions on Magnetics,* vol. 46, no. 12, pp. 4066-4072, 2010.

[8] I. Petrov, Y. Liu, V. Abramenko, P. Lindh, and J. Pyrhönen, "Direct-on-line-start permanent-magnet-assisted synchronous reluctance machine with ferrite magnets," in *IECON 2017-43rd Annual Conference of the IEEE Industrial Electronics Society*, 2017, pp. 1911-1918: IEEE.

[9] H. Liu and J. Lee, "Optimum Design of an IE4 Line-Start Synchronous Reluctance Motor Considering Manufacturing Process Loss Effect," *IEEE Transactions on Industrial Electronics,* vol. 65, no. 4, pp. 3104-3114, 2018.

[10] H. Kim, Y. Park, H.-C. Liu, P.-W. Han, and J. Lee, "Study on Line-Start Permanent Magnet Assistance Synchronous Reluctance Motor for Improving Efficiency and Power Factor," *Energies,* vol. 13, no. 2, p. 384, 2020.

[11] S. Baka, S. Sashidhar, and B. G. Fernandes, "Design and Optimization of a Two-Pole Line-Start Ferrite Assisted Synchronous Reluctance Motor," in *2018 XIII International Conference on Electrical Machines (ICEM)*, 2018, pp. 131-137.

[12] A. Jamali Fard and M. Mirsalim, "A robust numerical method for drawing the fluid flux-barrier geometry in the inner and outer rotor radial flux synchronous reluctance machines based on the finite difference method," *COMPEL - The international journal for computation and mathematics in electrical and electronic engineering,* vol. ahead-of-print, no. ahead-of-print, 2022.

[13] C. López-Torres, A. Garcia, J. Riba, G. Lux, and L. Romeral, "Computationally Efficient Design and Optimization Approach of PMa-SynRM in Frequent Operating Torque–Speed Range," *IEEE Transactions on Energy Conversion,* vol. 33, no. 4, pp. 1776-1786, 2018.

[14] F. Cupertino, G. Pellegrino, and C. Gerada, "Design of Synchronous Reluctance Motors With Multiobjective Optimization Algorithms," *IEEE Transactions on Industry Applications,* vol. 50, no. 6, pp. 3617-3627, 2014.

[15] A. Jamali Fard and M. Mirsalim, "An adaptive method for calculation of iron losses in switched reluctance motors using a minimum number of magnetostatic finite element simulations," *COMPEL - The international journal for computation and mathematics in electrical and electronic engineering,* vol. 41, no. 5, pp. 1566-1583, 2022.